Phys. Status Solidi RRL **7**, No. 10, 781–792 (2013) / **DOI** 10.1002/pssr.201307253

Part of Focus Issue on
Semiconductor Nanowires
Eds.: Chennupati Jagadish, Lutz Geelhaar, Silvija Gradecak

pss +++rapid research letters+++
www.pss-rapid.com

Review@RRL

Nanofunctional gallium oxide (Ga_2O_3) nanowires/nanostructures and their applications in nanodevices

Sudheer Kumar* **and R. Singh****

Department of Physics, Indian Institute of Technology Delhi, Hauz Khas, New Delhi-110016, India

Received 1 June 2013, revised 2 August 2013, accepted 5 August 2013
Published online 15 August 2013

Keywords gallium oxide, nanowires, vapor–solid–liquid growth, luminescence, SEM, TEM

* Corresponding author: e-mail sudheer83.iitr@gmail.com, Phone: +91 2659 6658
** e-mail rsingh@physics.iitd.ac.in, Phone: +91 2659 6495

A brief review on beta gallium oxide (β-Ga_2O_3) nanowires (NWs) and nanostructures (NS) is presented in this article. β-Ga_2O_3 is a wide-bandgap ($E_g \sim 4.9$ eV) semiconductor and can be doped with n- and p-type dopants, which can lead to applications in many functional devices. Here, we will first discuss briefly the properties of β-Ga_2O_3 in bulk form. Then we will describe the growth of β-Ga_2O_3 NWs/NS using various techniques including thermal CVD, MOCVD and laser ablation. The present status of research in the area of nanowire growth will be highlighted in this section. Then we will describe the luminescence properties of β-Ga_2O_3 NWs such as photoluminescence (PL) and cathodoluminescence (CL). The origin of various peaks in the PL and CL spectra of β-Ga_2O_3 NWs/ NS will be presented, with reference to various experimental studies carried out recently. In the final section, we will describe various applications of β-Ga_2O_3 NWs in nanodevices such as field effect transistors (FET), gas sensors and deep-UV photodetectors. Finally, we will give a conclusion and future perspective of the research in the area of this important semiconducting oxide.

1 Introduction Gallium oxide is an important semiconducting oxide and has a resemblance to alumina (Al_2O_3) [1]. It was first studied in 1950 and its crystal structure was explored in 1960 by Geller [2]. The optical properties of Ga_2O_3 were found to be similar to ruby. The five phases of Ga_2O_3 named as α-, β-, γ-, δ-, and ε exist in nature depending upon preparation conditions [3]. Among all of these phases, β-phase is the thermally and chemically most stable, while all other phases are in a metastable state and transform into β-phase at high temperature (more than 600 °C). The β-Ga_2O_3 has a wide bandgap ~4.9 eV [4, 5] at room temperature (RT). Initially, it was assumed that β-Ga_2O_3 is an intrinsically n-type semiconductor due to shallow donor negative oxygen vacancies with an ionization energy around 30–40 meV [6]. These oxygen vacancies are mostly responsible for conduction [6] as well as luminescence [7] in the β-Ga_2O_3. But recently, Villora et al. [8] investigated that Si is an effective n-type dopant for β-Ga_2O_3. Both electrical conduction and free-carrier concentration can be intentionally changed up to three orders of magnitude by Si doping. They suggested that the main impurity present in Ga_2O_3 powders is Si, and therefore, the above assumption for an impurity-band conduction created only by oxygen-vacancy donors is not sustainable, at least in the considered conduction range. In addition, Varley et al. [9] also investigated the influence of oxygen vacancy and other impurities on the electrical and optical properties of Ga_2O_3. They found that oxygen vacancies cannot explain the observed unintentional n-type conductivity, because they are deep donors with an ionization energy of about 1 eV. They also explored other dopants such as Si, Ge, Sn, F, and Cl, which behave like shallow donors.

β-Ga_2O is attracting tremendous research interest as a potential candidate in various fields including transparent conducting oxide (TCO), flat-panel display, solar-cell energy conversion, ultraviolet (UV) limiters, high-temperature gas sensors and as antireflection coatings [10–15]. In recent decades, low-dimensional β-Ga_2O_3 structures in-

cluding NWs, nanobelts, nanorods, and nanosheets have attracted growing attention of researchers due to their superior properties as compared to their bulk counterpart. One very important advantage of β-Ga_2O_3 NWs is their large surface to volume ratio providing more surface states to interact with the surroundings. Due to the wide bandgap, a large number of defect states are available inside the β-Ga_2O_3 NS; hence it emits a wide range of defect emissions from the infrared to the UV due to these defect states [16–35]. The luminescence properties of undoped and doped β-Ga_2O_3 have been studied in the form of bulk [16–21] and NS [21–35] earlier.

In the literature, various synthesis techniques have been employed to grow β-Ga_2O_3 NWs/NS [49–80] including thermal evaporation by evaporating a bulk gallium target under controlled conditions, laser-ablation growth occurs without a catalyst, arc-discharge by electrical discharge of GaN powders mixed with small amount of transition metals, thermal chemical vapor deposition (CVD) by evaporating pure gallium metal as a Ga vapor source under different conditions in a tubular furnace, carbothermal reduction, metalorganic CVD (MOCVD) using a single-source organometallic precursor at low temperature, microwave plasma, and so on. Some details of these methods will be discussed in a later section that is devoted to the growth of β-Ga_2O_3 NWs/NS.

In recent years, many novel nanoscale devices have been constructed using β-Ga_2O_3 NWs including FETs, gas sensors, photodetectors, and nanophotonic switches. To the best of our knowledge, no review article exists that provides complete information about the β-Ga_2O_3 NWs/NS synthesis techniques, luminescence properties, and their application in nanodevices.

This article provides a brief review on the recent research activities of β-Ga_2O_3 NWs and NS including growth techniques, luminescence properties, and their applications in nanodevices. The article is divided into four main sections. The first section introduces crystal structures and electronic band structure of bulk β-Ga_2O_3. In the second section, we will discuss the growth techniques used to grow β-Ga_2O_3 NWs/NS in the literature. In the third section, we will discuss the luminescence properties of β-Ga_2O_3 NWs/NS including PL and CL. The origin of various peaks in the PL and CL spectra of β-Ga_2O_3 NWs/NS will be discussed. In the final section, we will describe β-Ga_2O_3 NWs based nanodevices such as FETs, gas sensors and deep-UV photodetectors.

2 Properties of β-Ga_2O_3

In this section, we will discuss the crystal structure and electronic band structure of β-Ga_2O_3 and then summarize the main properties of this material.

2.1 Crystal structure

As we have mentioned in the Introduction, the crystal structure of Ga_2O_3 was first examined by Geller [2]. Further, Åhman et al. [36] and Janowitz et al. [37] also discussed the crystal structure of β-Ga_2O_3. The β-form (monoclinic structure) of Ga_2O_3 is the most thermally stable from RT to the melting point. The other forms are in metastable states and convert into the β-form at sufficiently high temperature. It is also chemically stable and there are only a few reports available that show the etching behavior of Ga_2O_3 single crystal [38]. β-Ga_2O_3 belongs to the C2/m space group and has base-centered monoclinic structure with lattice parameters $a = 12.23$ Å, $b = 3.04$ Å, $c = 5.80$ Å and $\beta = 103.7°$ (angle between 'a' and 'c' axes) and four Ga_2O_3 formula units per 20-atom unit cell [36]. In a unit cell, two nonequivalent Ga atoms [Ga(I) and Ga(II)] and three nonequivalent O atoms [O(I), O(II) and O(III)] are situated at 4i(x, 0, z) positions, at a symmetry plane (Fig. 1C). The Ga atoms have tetrahedral- and octahedral-like coordinations in the lattice. These crystalline structures are GaO_6 octahedra and GaO_4 tetrahedra: the zigzag double chains of edge-sharing GaO_6 octahedra are linked by single chains of vertex-sharing GaO_4 tetrahedra along the b-axis [Fig. 1(C)]. The oxygen ions are arranged in a distorted cubic close-packed array and three nonequivalent oxygen ions in the unit cell as shown in Fig. 1A.

Sudheer Kumar is a research scholar in the Department of Physics at Indian Institute of Technology Delhi, India. He received his B.Sc from CCS University, Meerut, India in 2005. He received his M.Sc in Physics and MTech. in Solid State Electronic Materials (SSEM) from Indian Institute of Technology, Roorkee, India in 2008 and 2010, respectively. His research focuses on the synthesis, characterization and nanodevice applications of semiconductor nanowires.

Rajendra Singh is an Associate Professor in the Department of Physics at Indian Institute of Technology Delhi, India. He received his Ph.D. in Physics from Inter-University Accelerator Centre (IUAC), Jawaharlal Nehru University, New Delhi, India in 2001. His Ph.D. work was concerned with the study of the effect of swift heavy ion irradiation on the electrical properties of Si and GaAs. After that he worked as a post-doctoral fellow at the Walter Schottky Institute, Technical University Munich, Germany from October 2001 to December 2003. There he worked on the design, fabrication and characterization of InP-based heterojunction bipolar transistors. From January 2004 to November 2006, he worked at the Max Planck Institute of Microstructure Physics, Halle, Germany. He was involved in the area of semiconductor wafer bonding, stained silicon-on-insulator (sSOI) fabrication and hydrogen-implantation-induced layer splitting studies in SiGe, GaN, InP and ZnO. His current research interests are semiconductor nanowires, nanolithography, GaN and related materials, effect of irradiation/implantation on semiconductors, etc. He has published about 70 publications in international journals. and edited volumes.

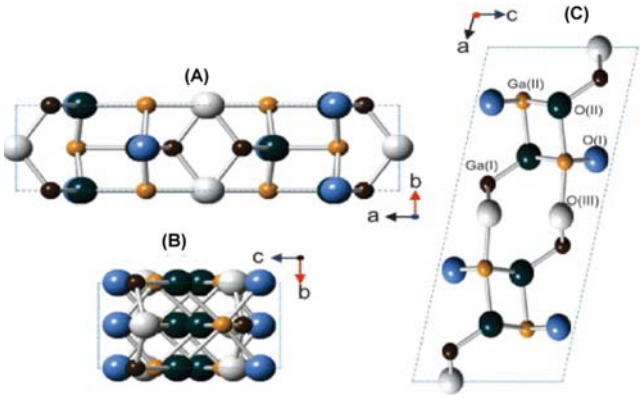

Figure 1 Unit cell of β-Ga_2O_3, which possesses two nonequivalent Ga sites: Ga (I), Ga (II) and three nonequivalent O-sites: O (I), O (II) and O (III). The Ga (I) sites have tetrahedral coordination, and the Ga (II) sites have octahedral coordination. Depicted is the projection of the unit cell of β-Ga_2O_3 along the *c*- (A), *a*- (B) and *b*-axis (C). [Reprinted with permission from C. Janowitz et al., New J. Phys. **13**, 085014 (2011). Copyright 2011, IOP Publishing Ltd. and Deutsche Physikalische Gesellschaft. Published under a CCBY-NC-SA Licence.]

2.2 Electronic band structure The first principle calculations were used to calculate the electronic band structure of β-Ga_2O_3 by many authors [9, 39, 40]. They used density functional theory (DFT) for calculating the band structure of β-Ga_2O_3. Yamaguchi [39] found that conduction-band minimum (CBM) in β-Ga_2O_3 was located at the gamma (Γ) point, while a valence-band maximum (VBM) was located at the E line. Therefore, β-Ga_2O_3 has an indirect bandgap of about 2.19 eV, which was underestimated due to local density approximation (LDA). Varley et al. [9] also observed an indirect bandgap of 4.83 eV, with VBM situated just off the M point, which was slightly smaller than the direct bandgap of 4.87 eV located at the Γ-point, as shown in Fig. 2. The estimated direct bandgap was consistent with previous experimental value of

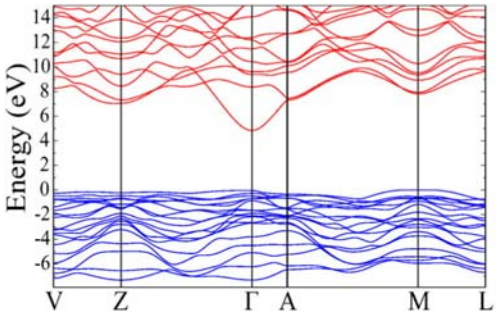

Figure 2 Electronic band structure of β-Ga_2O_3 calculated using the primitive unit cell of base-centered monoclinic β-Ga_2O_3. The VBM occurs just off the M point and is only 0.03 eV higher than at the Γ-point, is set to zero on the energy axis. [Reprinted with permission from J. B. Varley, J. R. Weber, A. Janotti, and C. G. Van de Walle, Appl. Phys. Lett. **97**, 142106 (2010). Copyright 2010, American Institute of Physics.]

Table 1 Summary of basic properties of β-Ga_2O_3.

S. N.	property	attributes
1	structure and space group	monoclinic and C2/m [2]
2	bandgap (E_g)	4.83 eV (indirect) and 4.87 eV (direct) at RT [39]
3	density	5.863 g/cm^3
4	dopants (n/p type)	Ti/Zn, Ge, Mg [41]
5	electron affinity (χ)	3.50 eV [42, 43]
6	refractive index (n)	1.9 [44, 45]
7	melting point	1800 °C [46]
8	electron effective mass	$0.342m_e$ [39]
9	electron mobility (μ_e)	10 cm^2 V^{-1} s^{-1} [46]
10	carrier density	10^{13}–10^{16} cm^{-3} [46]
11	rel. dielectric constant (ϵ)	10 [47]

~4.9 eV [7]. The works [9, 39, 40] concluded that β-Ga_2O_3 is an indirect bandgap, but effectively a direct bandgap material.

The main properties of β-Ga_2O_3 are summarized in Table 1.

3 Growth of Ga_2O_3 NWs and NS The β-Ga_2O_3 NS including NWs, nanosheets, nanobelts, nanorods and nanotubes have been synthesized using several techniques [49–81]. Here, in this section, we will first discuss about the growth mechanism involved in the formation of NS, and then give the description of various growth techniques including structural and morphological characterization of β-Ga_2O_3 NS. In the literature, these NS are grown via two well-known growth mechanisms: vapor–liquid–solid (VLS) and vapor–solid (VS). The VLS mechanism was first introduced by Wagner and Ellis in 1960 [48] that they observed in the growth of Si whiskers. In the case of the VLS mechanism, a foreign catalyst is required for the nucleation sites of nanowire growth. The interfacial energy, growth direction, and diameter of NWs are governed by these nucleation sites. Hence, a proper choice of catalyst is an important factor in this mechanism. The noble metal gold (Au) is used commonly as a catalyst, and various transition metals such as nickel (Ni), cobalt (Co), and iron (Fe) are also employed in the NWs growth. The catalysts are incorporated in the final product and hence is disadvantageous in nanoelectronic devices where accurate doping is required. In the case of the VS growth mechanism, no foreign catalyst is required and hence the NS are pure. These NS condense directly from source-rich vapor (kept at very high temperature) on the substrate (kept at low temperature region). By the VS growth mechanism, NWs, nanobelts and nanosheets are commonly formed, whereas by the VLS mechanism, only NWs are formed.

3.1 Physical evaporation This is a very simple technique and does not need sophisticated equipments. Zhang et al. [49] were the first to synthesize Ga_2O_3 NWs using physical evaporation. The authors found NWs on the

inner wall of the quartz boat that was used for Ga as a source material. The average diameter and length of as-grown NWs were ~100 nm and up to 100 μm, respectively. The X-ray diffraction (XRD) pattern of Ga_2O_3 NWs revealed a most intense peak at (400), while in the case of bulk Ga_2O_3, it was at (111). They suggested that this shifting in the peak position might be due to a size effect and disorder arising from NWs. The high-resolution transmission electron microscopy (HRTEM) results revealed that NWs had monoclinic crystal structure and the lattice spacing was around 0.28 nm, corresponding to (002) planes. These NWs were formed via the VS growth mechanism.

The fabrication of Ga_2O_3 NS was reported by many authors [50–52] via this method. They used GaN powder [50] or Ga metal [52] as a raw material and Indium (In) [50] or Au [52] as a catalyst on sapphire [50] or Si [52] substrates. In Ref. [50], the reaction occurred at 960 °C for 1 h under a constant flow of Ar and O_2 (4 : 1). The diameter of these NWs varied from 20 nm to 60 nm and length was up to several hundred micrometers. HRTEM results shown that the growth direction of as-grown NWs was [135] and the lattice d spacing between the $(21\bar{1})$ planes was 0.243 nm. In addition, the effect of Au-film thickness on the shape of NS was investigated by Guha et al. [52]. The nanoparticles size increased with increasing Au film thickness. Similar behavior was observed in the growth of ZnO NWs by Huang et al. [53]. They observed that the diameter of nanowire influenced the emission characteristics.

3.2 Arc-discharge This technique is useful for mass production of Ga_2O_3 NWs and has an inexpensive installation. However, one disadvantage of this technique is impurities in the product due to the tremendous production scale. Generally, in this method, graphite electrodes 6 mm in diameter and 10 cm in length are used as anodes. A small hole (diameter: 2 mm and depth: 10 mm) [54], (diameter: 4 mm and depth: 25 mm) [55] was drilled and filled with a mixture of GaN, graphite, and nickel powder. The cathode was a graphite rod with a diameter of 12 mm. Both anode and cathode holders were water cooled. A DC current 55–65 A (13–15 V) [55, 56], 25–30 A (35–45 V) [54] was applied between two electrodes under a total pressure of 400–500 Torr ($P_{Ar}:P_{O_2} = 400:100$). The duration of the process depended on plasma stability, and was generally 5–10 min. NWs were deposited on the cathode, chamber walls, and in between in the form of a web-like network.

Han et al. [54], Choi et al. [55] and Park et al. [56] investigated the growth of Ga_2O_3 NWs using this method. In Ref. [56], they mixed GaN powder with a small amount of transition metals [Ni and Co (Ni : Co = 1 : 1)] and pressed this into a small hole as mentioned above. The product was collected from the cathode. The NWs were not formed at pressures below 450 Torr and without additive transition metals, which suggested that a critical amount of oxygen gases pressure and transition metals were necessary to form Ga_2O_3 NWs. It was observed that the relative intensity of the most intense XRD peak was different for bulk and NWs, and the reason might be similar, as discussed previously [49]. The diameter and length of NWs was ~15–45 nm and up to 100 μm, respectively. XRD, HRTEM, and Raman results revealed that as-synthesised Ga_2O_3 NWs were single-crystalline monoclinic in nature.

3.3 Laser ablation This method is useful for high-quality production of Ga_2O_3 NS with low output and it needs expensive equipments. In laser ablation, generally a laser beam is employed for ablation of the Ga_2O_3 target.

The synthesis of β-Ga_2O_3 NWs using the laser-ablation method was reported by Hu et al. [57]. A beam of a KrF excimer pulse laser (λ = 248 nm, 34 nm pulse width, 10 Hz frequency, and power 350 mJ per pulse) was employed to ablate the Ga_2O_3 target. The distance between target and alumina substrate was ~6 cm. A mixture of gas flow (Ar and 5% H_2) and vacuum of 760 Torr was maintain inside the tube during the process. The NWs were deposited on alumina substrates at 800 °C for 5 h. The diameter of the as-grown NWs was varied in the range 15–50 nm and the length up to several μm. The VS growth mechanism was involved for the growth of β-Ga_2O_3 NWs. HRTEM and SAED patterns demonstrated that growth of nanowire was along [010] direction. The distance between lattice fringes was 0.28 nm, corresponding to $(\bar{2}02)$ planes. In addition to NWs, a few NWs also appeared as ring-shaped structures.

The main advantage of laser ablation technique is its versatility, because the composition of the nanowires can be varied by simply changing the composition of the laser ablation target.

3.4 Carbothermal reduction (CTR) The carbothermal reduction method is extremely promising for mass production. One major drawback of this method is high levels of carbon impurity in the final product. In this method carbon is used as reducing agent. The carbothermal reactions produce carbon monoxide (CO) and carbon dioxide (CO_2) as following reactions:

$$C + O_2 \rightarrow CO_2 , \quad (1)$$

$$2C + O_2 \rightarrow 2CO . \quad (2)$$

The reaction (1) takes place at lower temperature (below 650 °C), while reaction (2) is favored at higher temperature.

Wu et al. [58] reported synthesis of Ga_2O_3 NWs by carbothermal reduction reaction. They mixed Ga_2O_3 powders with graphite in the ratio of 1 : 1.5 and ground for 1 h. Then, the mixture was put in an alumina boat covering with ceramic plates and placed inside the center of the tube furnace at 980 °C for 2 h under a constant flow of N_2 (20 ml/min). The wool-like product was deposited on the inner wall of the alumina boat and ceramic plate. The average diameter of as-synthesized NWs was ~60 nm and the length was up to many micrometers. The SAED pattern revealed the growth of NWs along the $[0\bar{1}1]$ direction.

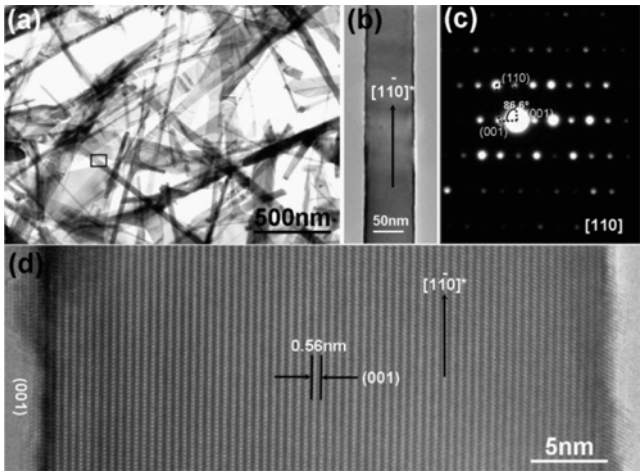

Figure 3 (a) Low-magnification TEM images of β-Ga_2O_3 nanoribbons, (b) TEM image of β-Ga_2O_3 nanoribbon grown along the [1 $\bar{1}$0] direction, (c) SAED pattern of β-Ga_2O_3 nanoribbon shown in part (b), (d) HRTEM image of β-Ga_2O_3 nanoribbon in part (b). [Reproduced with permission from G. X. Wang, J. Park, X. Y. Kong, P. R. Wilson, Z. X. Chen, and J. H. Ahn, Cryst. Growth Des. **8**, 1940–1944 (2008). Copyright 2008, American Chemical Society.]

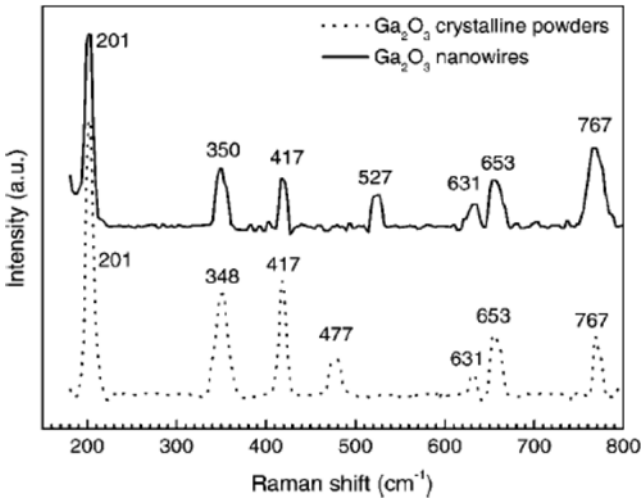

Figure 4 Raman spectra of the β-Ga_2O_3 nanowires and crystalline powder. [Reprinted with permission from G. X. Wang, J. Park, X. Y. Kong, P. R. Wilson, Z. X. Chen, and J. H. Ahn, Cryst. Growth Des. **8**, 1940–1944 (2008). Copyright 2008, American Chemical Society.]

Furthermore, various types of NS such as NWs, nanosheets, nanobelts and nanoribbons were synthesized successfully using this approach [59–61]. In their synthesis process, Wang et al. [61] mixed Ga_2O_3 powder with carbon black (1 : 1) and put into an alumina boat that was placed in a three temperature zone furnace. In the furnace, the Si wafer and quartz substrates (800–900 °C) were placed at different distances from the source material (1000 °C). HRTEM results confirmed that these NS consist of single-crystalline monoclinic structure. It has been observed that β-Ga_2O_3 NWs were grown in the high temperature zone (900 °C), while nanosheets and nanoribbons were formed in the medium temperature zone (800 °C) in low-pressure environments. Figure 3a shows the low magnification TEM image of β-Ga_2O_3 nanoribbons. Figure 3b shows a magnified TEM image of nanoribbon (width 80 nm), which is framed in Fig. 3a. The SAED pattern of this nanoribbon was recorded along the [110] zone axis (Fig. 3c). The growth direction was [1 $\bar{1}$0] as shown in Fig. 3(d). The Raman spectra as shown in Fig. 4 reveal that NWs have good monoclinic crystalline nature and match well with previous reports [62, 63].

3.5 CVD and MOCVD Chemical vapor deposition (CVD) is a most promising method for industrial scale up due to its relatively low growth temperature and high purity with high yield among all the methods. It is divided into two parts such as low (growth temperature lower than 700 °C) and high temperature (above 700 °C) CVD. The main advantage of high-temperature CVD is the much broader choice of possible VLS catalyst materials other than Au. On the other hand, the advantages of low-temperature CVD are that NWs with a large variety of diameters and lengths can be grown epitaxially on substrates. There are many reports where Ga_2O_3 NS/NWs were fabricated using CVD method [64–77]. The schematic diagram of a typical CVD system is shown in Fig. 5. In the CVD technique, Ga is evaporated at the middle of furnace and the Ga vapors are transferred over the substrate using some carrier gas.

Li et al. [64], Chang and Wu [65] and Dai et al. [66] reported synthesis of Ga_2O_3 NS by this technique. In their synthesis process, the Ga vapor reacted with H_2O at 700–950 °C on silicon [64, 66] or alumina [65] substrates. The following reaction occurred:

$$2Ga + 3H_2O \rightarrow Ga_2O_3 + 3H_2 \,. \qquad (3)$$

This reaction was carried out in a quartz tube that was inserted into a tubular furnace. In Ref. [65], they achieved a remarkable reduction of the diameter and increase in the length of the β-Ga_2O_3 NWs. They used a modified Ga vapor supply method for avoiding oxidation of the Ga

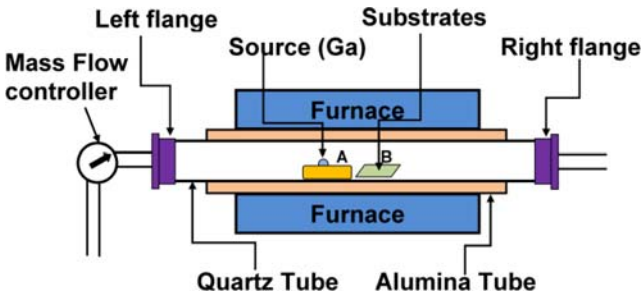

Figure 5 Schematic experimental setup for the growth of Ga_2O_3 NWs. Gallium metal and substrates were placed in quartz boats A and B, respectively.

metal source by separating the Ga vapor and H_2O before they reached the substrate. The diameter the as-grown NWs was in the range 20–40 nm. The lengths of the β-Ga_2O_3 NWs were 0.4–0.5 μm and 1.5–2.0 μm on average for 2 h and 6 h growth, respectively. TEM analysis indicated a single-crystalline structure nature of β-Ga_2O_3 NWs. The Ni-Ga-O alloy appeared at the end of nanowire, indicated a VLS growth mechanism. The SAED pattern recorded along the [010] zone axis and lattice *d* spacing was about 0.46 nm corresponding to the $(\bar{2}01)$ planes.

Another precursor such as a mixture of Ga and Ga_2O_3 has been used to grow Ga_2O_3 NWs with and without a catalyst by various groups [67–70]. In Ref. [69], Xiang et al. placed a mixture of Ga and Ga_2O_3 in molar ratio 4 : 1 inside the furnace at 1000–1200 °C under a constant flow of O_2 (500 sccm) for 1 h. The alumina substrate was coated with 0.01 M ethanol solution of $NiCl_2 \cdot H_2O$ for Ni nanoparticles as a catalyst. They also used uncoated substrates. When Ga and Ga_2O_3 mixed, Ga_2O (g) is created as

$$4Ga\ (l) + Ga_2O_3\ (s) \rightarrow 3Ga_2O\ (v)\ . \quad (4)$$

It has been proposed that without the catalyst, the reaction might be involved for NWs growth as

$$Ga_2O\ (g) + O_2\ (g) \rightarrow Ga_2O_3\ (s)\ . \quad (5)$$

When Ni was used as catalyst, the Ga_2O (g) would be deposited on Ni nanoparticle and dissolved into them. The continuous supply of Ga_2O (g) and O_2 (g) would be precipitated into Ga_2O_3 (s). The diameter of the NWs was 30–80 nm. The length of NWs grown without the catalyst was in between 10–20 μm and was shorter than those grown with the Ni catalyst (up to 500 μm). These NWs were single-crystalline monoclinic in nature. The NWs grown without a catalyst revealed some planar defects and were grown uniformly in the [010] direction, whereas the NWs grown with Ni catalyst were almost defect-free and randomly oriented.

In addition, various types of Ga_2O_3 NS including nanorods, nanoribbons, NWs, and cones have also been fabricated via this method [71–74]. Auer et al. [74] used metallic Ga and oxygen as sources. It was suggested that nanoribbons and rods were formed via a VS mechanism, whereas a VLS mechanism was responsible for NWs growth. The excellent epitaxial growth was observed for the NWs grown on sapphire substrates that mapped the hexagonal symmetry of (0001) sapphire.

Recently, Tien et al. [75] reported high-density monoclinic β-Ga_2O_3 NWs via a CVD method under a controlled ambient of oxygen. The structures and morphology were characterized by XRD, FE-SEM and HRTEM, as shown in Fig. 6. The XRD patterns of β-Ga_2O_3 NWs grown using CVD technique under different concentrations of O_2 are shown in Fig. 6a. The morphology of β-Ga_2O_3 NWs grown at 1% ambient oxygen can be seen in Fig. 6b. TEM images of a single β-Ga_2O_3 NWs and the corresponding SAED pattern recorded along the [110] zone axis are visible in Fig. 6c. High-resolution image of the lattice fringes are

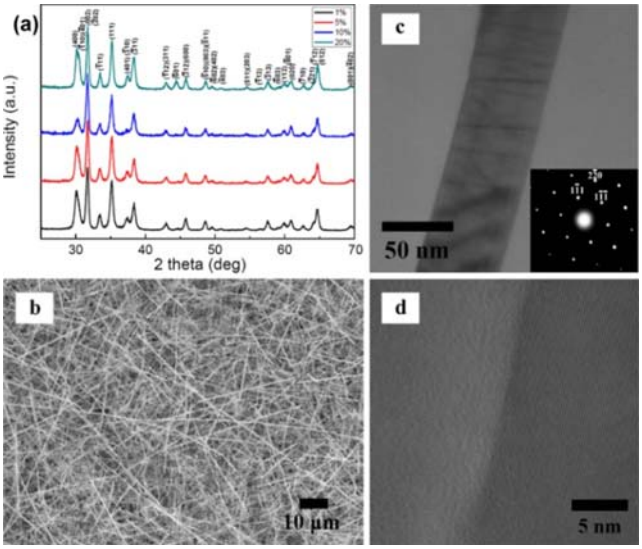

Figure 6 (a) The XRD pattern of β-Ga_2O_3 NWs grown under different concentrations of ambient oxygen; (b) SEM image of β-Ga_2O_3 NWs grown under 1% ambient oxygen; (c) TEM images of a single β-Ga_2O_3 NWs, the inset shows the SAED pattern; (d) high-resolution image of the lattice fringes. [Reprinted from L. C. Tien, C. H. Ho, X. T. Yao, and J. R. Cai, Appl. Phys. A **102**, 105–108 (2011). Copyright 2011, with permission from Springer.]

clearly depicted in Fig. 6d. HRTEM analysis indicates that the as-grown β-Ga_2O_3 NWs were single crystals with monoclinic structure, having grown in the $[1\bar{1}0]$ direction.

Low-temperature growth of β-Ga_2O_3 NWs on Au coated sapphire (0001) substrates at 550 °C under a constant N_2 flow was first time performed by Chang and Wu [76 (a) and (b)]. Thereafter, Kim et al. [77] also produced the large-scale β-Ga_2O_3 nanowire arrays on sapphire substrates using MOCVD. In Ref. [76], the organometallic precursor gallium acetylacetonate $(CH_3COCHCOCH_3)_3Ga$ [low decomposition temperature ~196 °C] was used as the single source for both Ga and O_2 and was placed at a low temperature in a two-temperature zone furnace. The well-aligned NWs were observed on sapphire substrate at 550 °C under a pressure of 100–500 Torr. A similar experiment was performed on Au-coated Si substrate but randomly oriented NWs were observed. The average diameter and length of NWs grown on sapphire for 30 min were 10 nm and 2.5 μm, respectively. They have also obtained well-aligned NWs in the $[\bar{2}01]$ direction on sapphire with diameter and length 10 nm and 4 μm for 60 min.

3.6 Microwave plasma This is a useful technique to grow NS on a large scale, through which rapid evaporation and decomposition of precursor materials result in NS of high purity. Moreover, it demonstrates good stability, uniform temperature field (controllable in a range of 300–900 °C) and normal ambient pressure. One most important advantage of this method is that it does not need any catalyst, which helps avoid the catalyst contamination. In

recent years, many groups have reported synthesis of β-Ga_2O_3 NWs via a microwave plasma method [78–80].

Sharma and Sunkara [78] demonstrated bulk synthesis of highly crystalline β-Ga_2O_3 tubes, NWs, and nanopaintbrushes by this technique. Later, Zhu et al. [79, 80] also demonstrated large-scale growth of β-Ga_2O_3 NWs. In Ref. [78], the synthesis was carried out in a microwave plasma reactor with a mixture of hydrogen (H_2)/methane (CH_4)/O_2. All the substrates were covered with a thin film of molten Ga and were exposed to a microwave plasma containing a range of gas-phase species. During plasma exposure, molten Ga flowed on all substrates, forming a thin film, which was followed by formation of a polycrystalline film along with some sparse NWs. The experimental conditions were microwave power of 600–1200 W, pressure of 30–60 Torr, growth time of 1–12 h, 0.6–10 sccm of O_2/0–2 sccm of CH_4 in 100 sccm of H_2 in the feed gas. The diameters of NWs were about of 20–100 nm, while their lengths were tens to hundreds of micrometers. The nanowire was grown along the [110] direction. They postulated three basic steps for the nucleation and growth of oxide nanowires. Furthermore, this proposed three-step mechanism was analyzed with thermodynamic arguments.

In summary, in spite of a large number of studies presented in this growth section, controlled and vertical aligned growth of β-Ga_2O_3 NWs is rare and still a challenge, which needs further investigation. The selective growth of β-Ga_2O_3 nanowire, which is also not observed, can be achieved via catalyst patterning. Only a few reports related to oriented growth of β-Ga_2O_3 NWs using a MOCVD technique were observed, so there is a need for other approaches. Moreover, Molecular beam epitaxial (MBE) and pulsed laser deposition (PLD) techniques could prove to be excellent approaches with controlled and uniform diameter as well as doping in β-Ga_2O_3 NWs/NS.

4 Luminescence properties of Ga_2O_3 NWs and NS The wide-bandgap nature of β-Ga_2O_3 provides the possibility of light emission from defect states between the infrared to ultraviolet regions of the spectrum. In recent decades, the luminescence properties of β-Ga_2O_3 have been studied in the form of bulk as well as NS. It emits blue, UV, green and red emission bands. The origin of all these emission bands (1.7–4.0 eV) has been suggested by several authors [16–35]. UV emission (3.45 eV) was independent of dopant and growth conditions. The origin of UV emission is related to recombination of self-trapped excitons [recombination of an electron and a hole from the lowest oxygen vacancy level to the top of the valance band (VB)]. The green emission (2.37 eV) appears in the presence of some impurities such as Be, Ge, Sn, Li, Zr, and Si [17] and increases with the oxygen partial pressure of the growth environment in undoped samples [16, 19, 21]. The blue (2.67 eV) and deep blue (3.04 eV) emissions originate from recombination of an electron on defect donor states formed by oxygen vacancies (V_O) and a hole on an acceptor is formed by gallium vacancy (V_{Ga}) or a gallium–oxygen vacancy pair (V_O, V_{Ga}) (Binet and Gourier 1998 [7]; Harwig and Kellendonk 1978 [17]). Shimamura et al. [82] studied excitation and PL of pure and Si-doped β-Ga_2O_3 single crystals. They observed UV-blue emission peaks when excited at two bands. In the case of the undoped sample, the feature of spectra was independent of the excitation and emission wavelengths. While, in the case of the Si-doped sample, the blue emission was strongly dependent on the excitation and emission wavelength. Moreover, in 2004 and 2011, Song et al. [83] and Chang et al. [84], respectively, observed red emission and they suggested that this was due to the presence of nitrogen impurity. Here, in this present section we discuss the luminescence properties of Ga_2O_3 NWs including PL and CL.

4.1 PL spectra of Ga_2O_3 NWs The PL spectra of undoped and doped bulk Ga_2O_3 have been widely studied by many authors [16–21]. Binet and Gourier [7] studied PL spectra of undoped Ga_2O_3 single crystal. They observed blue emission and showed the temperature effect on this blue emission. The intensity of the blue emission decreased with an increase in the temperature. They proposed a model for the PL emission mechanism of bulk Ga_2O_3 single crystal. According to this model, the blue emission process occurred when an electron in a donor cluster creating a donor band is captured through a tunnel transfer by a hole on an acceptor to form trapped excitons and these excitons recombine radiatively to emit a blue photon. In recent years many researchers have studied PL spectra of Ga_2O_3 NWs. Recently, Jangir et al. [85] studied the PL spectra of β-Ga_2O_3 NS annealed in different environments (oxygen, water vapor and ammonia solution). They synthesized β-Ga_2O_3 NS on Si substrate, and divided this substrate into four pieces. Figure 7 shows the RT-PL spectra

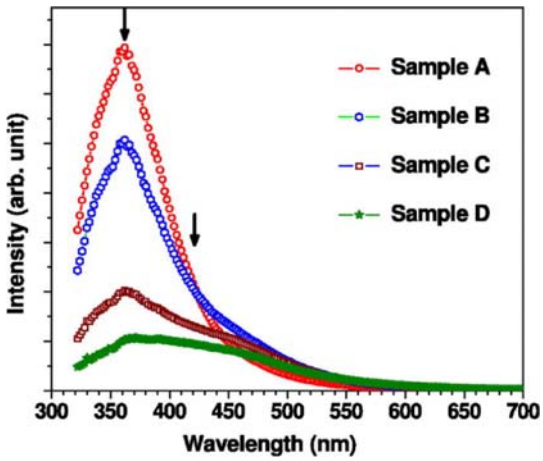

Figure 7 RT-PL spectra of β-Ga_2O_3 nanostructure samples A, B, C, and D that is sensitive to the annealing under different environments [Reprinted with permission from R. Jangir, S. Porwal, P. Tiwari, P. Mondal, S. K. Rai, T. Ganguli, S. M. Oak, and S. K. Deb, J. Appl. Phys. **112**, 034307 (2012). Copyright 2012, American Institute of Physics.]

of β-Ga_2O_3 NS samples A, B, C, and D [sample A was untreated, whereas samples B, C, and D were annealed under oxygen, water vapor, and ammonia, respectively], having a broad UV-blue emission peak centered at 360 nm in each sample. They extended the above model to explain the PL mechanism of β-Ga_2O_3 NS. According to this model, when an acceptor is excited with an excitation source a hole on the acceptor and electron on the donor are generated as the following equation shows:

$$(V_O, V_{Ga})' + V_O^{\bullet} + h\nu \rightarrow (V_O, V_{Ga})^X + V_O^X . \quad (6)$$

Also, the blue emission occurred via a reverse process of this. The electron is detrapped from the donor to the conduction band according to

$$V_O^X \rightarrow V_O^{\bullet} + e_{CB}^- , \quad (7)$$

while a hole may be detrapped from an acceptor to the valence band according to the equation

$$(V_O, V_{Ga})^X \rightarrow (V_O, V_{Ga})' + h'_{VB} . \quad (8)$$

According to the above model, the detrapped electron and holes gives the UV emission (~360 nm) via self-trapped excitons.

4.2 CL spectra of Ga_2O_3 NWs The CL investigation on undoped and doped bulk Ga_2O_3 has been carried out by several groups [24, 27, 28, 86, 87]. The CL emission mechanism is similar to the PL emission mechanism, which we have discussed in a previous section. Villora et al. [88] studied CL of undoped Ga_2O_3 single crystal. They observed five emissions in their CL spectra from UV-green wavelength. Nogales et al. [27] studied CL spectra from Ga_2O_3 NWs and observed the violet-blue emission band of Ga_2O_3 along with a red emission at 1.73 eV dominant in the NWs. Again in 2009, Nogales et al. [28] carried out a CL study of isoelectronic (In, Al) doped Ga_2O_3 NWs. They found that isoelectronic impurities changed the CL of Ga_2O_3 NWs. It has been observed that the UV-blue band in Al- and In-doped Ga_2O_3 NWs is blue shifted about 0.20 eV and 0.40 eV, respectively, when it was compared with undoped samples. Recently, Guzman-Navarro and his coworker [24] studied the CL spectra of Ga_2O_3 NWs and observed blue and UV emission. Figure 8 displays the CL spectra at 90 K and 300 K from sample 1 and 2, respectively [samples 1 and 2 were grown on Si(100) substrates at 250 °C (with a 7.8 sccm Ar flow rate for 4 h) and 360 °C (with a 30 sccm N_2 flow rate for 6 h), respectively], having a broad UV emission at 3.31 eV. It has been observed that thermal treatment of samples increased the UV emission and quenched the blue band. This quenching of the blue emission indicates that thermal treatment of the samples has eliminated the point defects that are mostly responsible for this emission. Similar behavior was observed by Nogales et al. [27], who also noticed an increase in intensity of UV band when treated thermally at 1500 °C for 24 h.

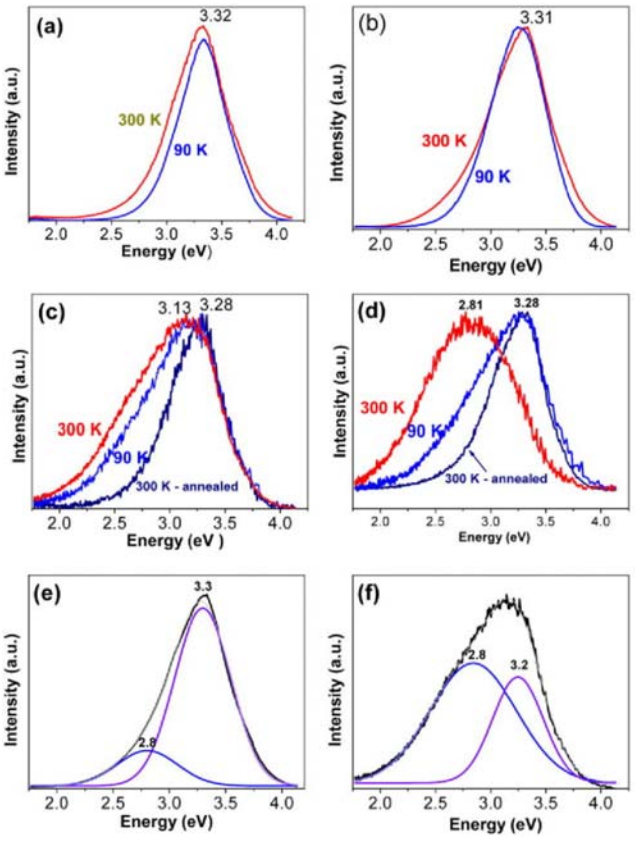

Figure 8 Normalized CL spectra of β-Ga_2O_3 NWs obtained at 90 K and 300 K from (a)–(d) samples 1–4, respectively. Deconvoluted CL spectrum acquired at 300 K from the (e) sample 1 and (f) the sample 3 [Reprinted with permission from G. Guzman-Navarro, M. Herrera-Zaldivar, J. Valenzuela-Benavides, and D. Maestre, J. Appl. Phys. **110**, 034315 (2011), Copyright 2011, American Institute of Physics.]

5 Applications of Ga_2O_3 NWs Semiconductor Ga_2O_3 NWs, nanobelts and nanorods have been extensively studied in recent years. These Ga_2O_3 NS provide a path to a new generation of devices, but most Ga_2O_3 NS-based devices are limited to single-NW devices and to integrate all individual devices into a single unit chip is still a real challenge. Another crucial issue is controlled doping in NS and Ohmic contact between NS and the electrodes. Therefore, to construct a device via a simple and cost-effective method is still a grand challenge. In spite of all these issues, various Ga_2O_3 NWs applications such as Ga_2O_3 NWs based FETs, gas sensors and deep UV photodetectors are reported.

5.1 Ga_2O_3 NWs-based FET The Ga_2O_3 NWs-based FET was demonstrated by Zhao et al. [87] and Chang et al. [89]. They constructed a single Ga_2O_3 nanowire based FET to characterize the electrical properties of the as-grown NWs [88]. The device was fabricated by a thermally grown silicon dioxide (SiO_2) film with 500 nm thickness on the top of n-type silicon (Si) wafers, followed by deposition of

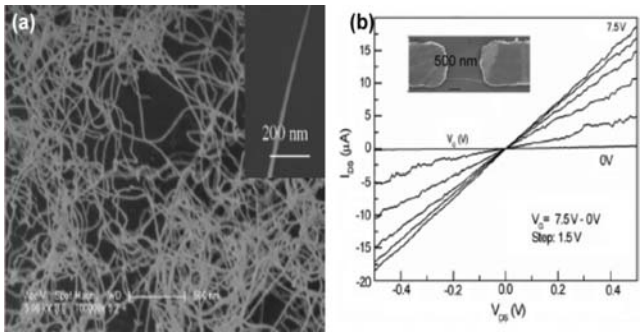

Figure 9 (a) High-magnification SEM images of Ga_2O_3 NWs and inset shows the TEM image of a single nanowire, (b) I–V characteristics were recorded at different gate voltages for a single Ga_2O_3 nanowire FET. The inset is the SEM image of the as-fabricated single Ga_2O_3 nanowire FET, the scale bar is 500 nm. [Reprinted from Z. Li, B. Zhao, P. Liu, and Y. Zhang, Microelectron. Eng. **85**, 1618–1620 (2008). Copyright 2008, with permission from Elsevier.]

Au metal via sputtering and standard optical lithography. Parallel Au-electrode pairs (length ~10 μm and thickness ~80 nm) were patterned. The parallel Au electrodes (the distance between two electrodes was ~2 μm) were used as source and drain, and an n-type Si layer served as the back gate. The as-prepared Ga_2O_3 NWs were first ultrasonically dispersed in ethanol, and then the ethanol dispersions were dried onto an n-type silicon chip covered with 500 nm of SiO_2 with predefined Au electrodes. Figure 9a shows an SEM image of the grown NWs and the inset shows the TEM image of an individual nanowire. Figure 9b shows the current–voltage (I_{DS}–V_{DS}) data of the device. The gate voltages (V_G) were applied from 0 V to 7.5 V and the drain voltages were from –0.5 V to 0.5 V for RT samples. It is very clearly observed that the conductance increased with an increase in the back gate voltage, indicating n-type semiconductor characteristics of the Ga_2O_3 nanowire. The possible reason is due to oxygen vacancies and extra gallium interstitial atoms in the lattice during the synthesis process. An on-off current ratio ($I_{on}/I_{off} \geq 10^5$) has been achieved at V_G from 0 V to 7.5 V with V_{DS} of –0.2 V. The measured mobility of the channel was calculated (~65.4 cm^2/V s) from the relationship

$$g_m = \mu_e \left(\frac{C}{L^2}\right) V_{DS}\,, \tag{9}$$

where C is capacitance and L is length of channel, while g_m the transconductance and can be expressed as

$$g_m = \frac{dI_{DS}}{dV_G}\,. \tag{10}$$

The capacitance was calculated as

$$C = \frac{2\pi\,\varepsilon\varepsilon_0 L}{\ln\left(\frac{2h}{r}\right)}, \tag{11}$$

where $\varepsilon = 3.9$ and $h = 500$ nm are the dielectric constant and the thickness of the SiO_2 layer, respectively and r is the nanowire radius. The mobility of the Ga_2O_3 nanowire is comparable to previously reported GaN NWs.

5.2 Ga_2O_3 NWs-based gas sensors In the literature, Ga_2O_3 NWs-based gas sensors have been fabricated by many authors [90–93]. In order to construct a gas sensor, Arnold et al. [91] synthesized NWs (diameter ~20–100 nm) directly via a VLS method onto (sensor device) platinum interdigitated electrodes that were patterned by a photolithography technique. This interdigital comb-finger like structure (Fig. 10a) was used as a capacitive sensor. This sensor was inexpensive, easily fabricated and capable of detecting various analytes at RT. As a desired analyte passes over the nanowire mesh, the gas may be physisorbed onto defect sites of the nanowire surface. Therefore, a change in the device capacitance was noticed corresponding to a change in the dielectric constant of the mesh. The capacitance was increased with an increase in the concentrations of analyte vapors, as shown in Fig. 10c. Fast recovery of the sensing devices, without the use of an external heat source, allowed these devices to operate at low power.

5.3 Ga_2O_3 NWs-based photodetectors A single β-Ga_2O_3 nanowire- and nanobelt-based solar-blind photodetectors have been fabricated by Feng et al. [94] and Li et al. [95], respectively. Feng et al. [94] constructed a device structure of β-Ga_2O_3 NWs-based photodetector using photolithography. Two Au electrodes (thickness 50 nm) were deposited by e-beam deposition on silicon substrate with a 500 nm thick thermally grown SiO_2 layer. Then, a single nanowire was placed on the top of these electrodes. The measurements were carried out in a test chamber under a vacuum of 10^{-4} Torr. The upper inset of Fig. 11a shows an SEM image of as-synthesized NWs and the lower inset in Fig. 11a shows the single β-Ga_2O_3 nanowire-based device. The diameter and length of the used nanowire between two Au-electrodes were 40 nm and 400 nm, respectively. The current–voltage (I–V) characteristics of the photodetector device without and under a UV lamp with 254 nm (power 7 W) light illumination are shown in Fig. 11a and b, respectively. As the device was exposed to illumination by a UV lamp, its conductance greatly increased. The I–V characteristics of the device under illumination are asymmetric and nonlinear because of poor ohmic contacts between the Au-electrodes and the nanowire. Figure 11c and d show the real-time response of the detectors to 254 nm light by ON/OFF switching under a bias voltage of –8 V. It can be seen that the dark current is of the order of pA. After illumination, the current rapidly increases to several nA, but the current fluctuations are a little larger (maybe due to the surface species absorption/desorption or the appearance of defects). As the light is off, the current suddenly decreases to its original value. The upper limit of the response time, an up per limit of the

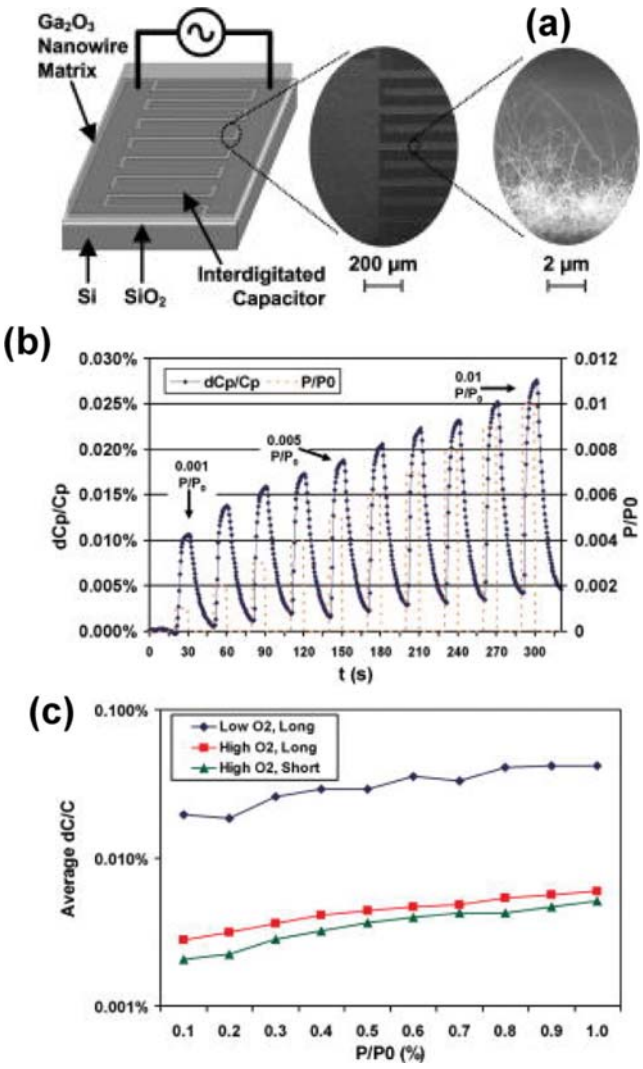

Figure 10 (a) Schematic diagram of the IDC sensor with a Ga_2O_3 nanowire dielectric sensing layer. (b) The capacitive response of an IDC sensor device to analyte pulses of 300–3000 ppm. (c) Average change in capacitance (dC/C) for analyte concentrations of 0.001 to 0.01P/P_0 for three device families: low O_2/long, high O_2/long, and high O_2/short, where low O_2 (high O_2) refers to relative quantities of oxygen defect sites, and long (short) refers to relative length of NWs. [Reprinted with permission from S. P. Arnold, S. M. Prokes, F. K. Perkins, and M. E. Zaghloul, Appl. Phys. Lett. **95**, 103102 (2009). Copyright 2009, American Institute of Physics.]

recovery time, and sensitivity were 0.22 s, 0.09 s, and ~1000, respectively.

6 Conclusions and future perspective This article provides a brief overview of the current status and achievements of Ga_2O_3 NWs/NS, ranging from synthesis and characterization to nanodevice applications. Due to its various interesting properties such as wide bandgap, chemical and thermal stability, ability to form a variety of NS, Ga_2O_3 could be of great importance for nanodevice applications in the coming years. Nanoscale FETs, nanostructure-based deep-UV photodetectors and nanosensors are some of these potential devices, where nanofunctional Ga_2O_3 could be of great advantage.

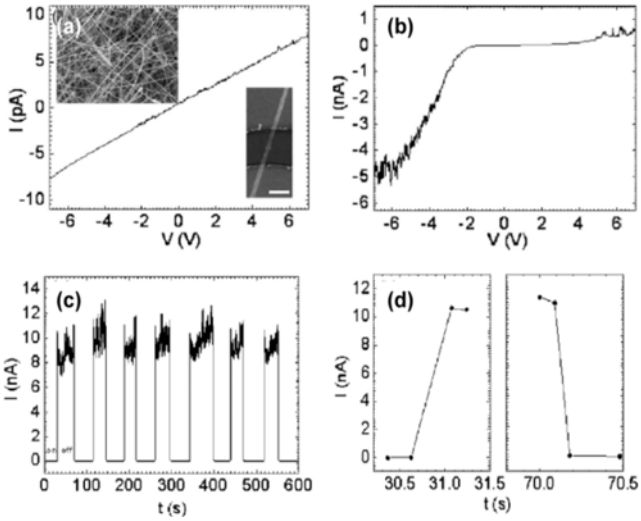

Figure 11 (a) and (b) I–V characteristics of the photodetector without and under 254 nm light illumination, respectively. The upper inset of (a) is an SEM image of NWs and the lower inset of (a) is a typical SEM image of the device (the scale bar: 200 nm). (c) Real-time photoresponse of the detector to 254 nm light. (d) Enlarged rise and decay edges for the first "ON" and "OFF", respectively. [Reprinted with permission from P. Feng, J. Y. Zhang, Q. H. Li, and T. H. Wang, Appl. Phys. Lett. **88**, 153107 (2006). Copyright 2006, American Institute of Physics.]

Despite significant progress in the area of Ga_2O_3 NWs/NS in the past ten years, there are still important issues that have to be improved/explored for the device applications of Ga_2O_3 NWs/NS. First, the applicability of semiconductor NWs depends on their electrical transport properties, which can be tuned by the introduction of controlled amounts of dopants in NWs. The aspect of intentional and unintentional doping of Ga_2O_3 NWs during growth is a major issue to be investigated for its device applications. Also, there is a need to improve the quality of Ohmic and Schottky contacts in Ga_2O_3 NWs. Finally, controlled and uniform assembly of NWs with high scalability is required and the integration of individual nanodevices into a circuit needs to be explored in the future.

In addition, there are various technical challenges that need to be addressed for the development of Ga_2O_3 NWs/NS such as (1) controlled and vertically aligned growth of Ga_2O_3 NWs/NS with uniform dimensions (length and diameter), (2) controlled doping in Ga_2O_3 NWs, (3) growth of radial core–shell and axial hetrostructures based on GIO (gallium indium oxide), (4) patterned and selective growth of Ga_2O_3 NWs, and (5) MBE, PLD and MOCVD could be promising techniques to grow controlled and vertically aligned Ga_2O_3 NWs and hetrostructures. Moreover, it is of utmost importance to understand the effect of various growth parameters on the optical,

structural and electrical properties of Ga_2O_3 NWs. The fabrication of high-quality nanodevices such as nano-FETs and nano-UV photodetectors using nanofunctional Ga_2O_3 is an area of research that should be pursued further in the future.

Acknowledgements Sudheer Kumar is thankful to IITD for providing a research fellowship. The authors are thankful to the Department of Electronics and Information Technology (DeitY), Government of India for providing financial support for this work.

References

[1] I. Levin and D. Brandon, J. Am. Cer. Soc. **81**, 1995–2012 (1998).
[2] S. Geller, J. Chem. Phys. **33**, 676–684 (1960); J. Solid State Chem. **20**, 209–210 (1977).
[3] R. Roy, V. G. Hill, and E. F. Osborn, J. Am. Chem. Soc. **74**, 719–722 (1952); Ind. Eng. Chem. **45**, 819–820 (1953).
[4] H. H. Tippins, Phys. Rev. **140**, A316 (1965).
[5] Z. Hajnal, J. Miro, G. Kiss, F. Reti, P. Deak, R. C. Herndon, and J. M. Kuperberg, J. Appl. Phys. **86**, 3792–3796 (1999).
[6] M. R. Lorenz, J. F. Woods, and R. J. Gambino, J. Phys. Chem. Solids **28**, 403 (1967).
[7] L. Binet and D. Gourier, J. Phys. Chem. Solids **59**, 1241 (1998).
[8] E. G. Villora, K. Shimamura, Y. Yoshikawa, T. Ujiie, and K. Aoki, Appl. Phys. Lett. **92**, 202120 (2008).
[9] J. B. Varley, J. R. Weber, A. Janotti, and C. G. Van de Walle, Appl. Phys. Lett. **97**, 142106 (2010).
[10] D. D. Edwards, T. O. Mason, F. Goutenoir, and K. R. Peoppel, Appl. Phys. Lett. **70**, 1706 (1997).
[11] M. Ogita, N. Saika, Y. Nakanishi, and Y. Hatanaka, Appl. Surf. Sci. **142**, 188–191 (1999).
[12] M. Ogita, K. Higo, Y. Nakanishi, and Y. Hatanaka, Appl. Surf. Sci. **175**, 721–725 (2001).
[13] M. Fleischer, S. Kornely, T. Weh, J. Frank, and H. Meixner, Sens. Actuators B **69**, 205–210 (2000).
[14] K. Shan, G. X. Liu, W. J. Lee, G. H. Lee, I. S. Kim, and B. C. Shin, J. Appl. Phys. **98**, 023504 (2005).
[15] M. Passlacki, E. F. Schubert, W. S. Hobson, M. Hong, N. Moriya, S. Chu, K. Konstadinidis, J. P. Mannaerts, M. L. Schnoes, and G. J. Zydzik, J. Appl. Phys. **77**, 686 (1995).
[16] G. Blasse and A. Bril, J. Phys. Chem. Solids **31**, 707 (1970).
[17] T. Harwig and F. Kellendonk, J. Solid State Chem. **24**, 255–263 (1978).
[18] T. Harwig, F. Kellendonk, and S. Slappendel, J. Phys. Chem. Solids **39**, 675–680 (1978).
[19] E. G. Villora, M. Yamaga, T. Inoue, S. Yabasi, Y. Mausi, T. Sugawara, and T. Fukuda, Jpn. J. Appl. Phys. **41**, L622–L625 (2002).
[20] E. G. Villora, K. Hatanaka, H. Odaka, T. Sugawara, T. Miura, H. Fukumura, and T. Fukuda, Solid State Commun. **127**(5), 385–388 (2003).
[21] E. G. Villora, T. Atou, T. Sekiguchi, T. Sugawara, M. Kikuchi, and T. Fukuda, Solid State Commun. **120**, 455–458 (2001).
[22] X. T. Zhou, F. Heigl, J. Y. P. Ko, M. W. Murphy, J. G. Zhou, T. Regier, R. I. R. Blyth, and T. K. Sham, Phys. Rev. B **75**, 125303 (2007).
[23] C. L. Kuo and M. H. Huang, Nanotechnology **19**, 155604 (2008).
[24] G. Guzman-Navarro, M. Herrera-Zaldivar, J. Valenzuela-Benavides, and D. Maestre, J. Appl. Phys. **110**, 034315 (2011).
[25] Z. X. Yang, F. Zhu, Y. J. Wu, W. M. Zhou, and Y. F. Zhang, Physica E **27**, 351–354 (2005).
[26] X. Xiang, C. B. Cao, Y. Guo, and H. S. Zhu, Chem. Phys. Lett. **378**(5–6), 660–664 (2003).
[27] E. Nogales, B. Mendez, and J. Piqueras, Appl. Phys. Lett. **86**, 113112 (2005).
[28] E. Nogales, B. Sanchez, B. Mendez, and J. Piqueras, Superlattices Microstruct. **45**, 156–160 (2009).
[29] E. Nogales, J. A. Garcia, B. Mendez, and J. Piqueras, Appl. Phys. Lett. **91**, 133108 (2007).
[30] E. Nogales, B. Mendez, J. Piqueras, and J. A. Garcia, Nanotechnology **20**, 115201 (2009).
[31] E. Nogales, J. A. Garcia, B. Mendez, and J. Piqueras, J. Appl. Phys. **101**, 033517 (2007).
[32] E. Nogales, B. Mendez, and J. Piqueras, Nanotechnology **19**, 035713 (2008).
[33] E. Nogales, B. Mendez, and J. Piqueras, Ultramicroscopy **111**, 1037–1042 (2011).
[34] J. Diaz, I. Lopez, E. Nogales, B. Mendez, and J. Piqueras, J. Nanopart. Res. **13**, 1833–1839 (2011).
[35] I. Lopez, A. D. Utrilla, E. Nogales, B. Mendez, J. Piqueras, A. Peche, J. Ramirez-Castellanos, and J. M. Gonzalez-Calbet, J. Phys. Chem. C **116**, 3935–3943 (2012).
[36] J. Áhman, G. Svensson, and J. Albertsson, Acta Crystallogr., Sect. C: Cryst. Struct. Commun. **52**, 1336 (1996).
[37] C. Janowitz, V. Scherer, M. Mohamed, A. Krapf, H. Dwelk, R. Manzke, Z. Galazka, R. Uecker, K. Irmscher, R. Fornari, M. Michling, D. Schmeisser, J. R. Weber, J. B. Varley, and C. G. Van de Walle, New J. Phys. **13**, 085014 (2011).
[38] S. Ohira and N. Arai, Phys. Status Solidi. **5**, 9 (2008).
[39] K. Yamaguchi, Solid State Commun. **131**, 739–744 (2004).
[40] H. Y. He, R. Orlando, M. A. Blanco, R. Pandey, E. Amzallag, I. Baraille, and M. Rerat, Phys. Rev. B **74**, 195123 (2006).
[41] Y. Cui, X. Duan, J. Hu, and C. M Lieber, J. Phys. Chem. B **104**, 5213–5216 (2000).
[42] T. Minami, T. Miyata, and T. Yamamoto, Surf. Coat. Technol. **583**, 108–109 (1998).
[43] I. Lopez, E. Nogales, P. Hidalgo, B. Mendez, and J. Piqueras, Phys. Status Solidi A **209**, 113 (2011).
[44] M. Rebien, W. Henrion, M. Hong, J. P. Mannaerts, and M. Fleischer, Appl. Phys. Lett. **81**, 250 (2002).
[45] M. Passlacki, E. F. Schubert, W. S. Hobson, M. Hong, N. Moriya, S. Chu, K. Konstadinidis, J. P. Mannaerts, M. L. Schnoes, and G. J. Zydzik, J. Appl. Phys. **77**, 686 (1995).
[46] M. Fleischer and H. Meixner, J. App. Phys. **74**, 300–305 (1993).
[47] M. Higashiwaki, K. Sasaki, A. Kuramata, T. Masui, and S. Yamakoshi, Appl. Phys. Lett. **100**, 013504 (2012).
[48] R. S. Wagner and W. C. Ellis, Appl. Phys. Lett. **4**, 89–90 (1964).
[49] H. Z. Zhang, Y. C. Kong, Y. Z. Wang, X. Du, Z. G. Bai, J. J. Wang, D. P. Yu, Y. Ding, Q. L. Hang, and S. Q. Feng, Solid State Commun. **109**, 677–682 (1999).

[50] J. Zhang and F. H. Jiang, Chem. Phys. **289**, 243–249 (2003).
[51] J. Zhang, Z. G. Liu, C. K. Lin, and J. Lin, J. Cryst. Growth **280**, 99–106 (2005).
[52] P. Guha, S. Chakrabarti, and S. Chaudhuri, Physica E **23**, 81–85 (2004).
[53] M. H. Huang, Y. Wu, H. Feick, N. Tran, E. Weber, and P. Yang, Adv. Mater. **13**, 113–116 (2001).
[54] W. Q. Han, P. Kohler-Redlich, F. Ernst, and M. Rühle, Solid State Commun. **115**, 527–529 (2000).
[55] Y. C. Choi, W. S. Kim, Y. S. Park, S. M. Lee, D. J. Bae, Y. H. Lee, G.-S. Park, W. B. Choi, N. S. Lee, and J. M. Kim, Adv. Mater. **12**, 746–750 (2000).
[56] G.-S. Park, W.-B. Choi, J.-M. Kim, Y. C. Choi, Y. H. Lee, and C.-B. Lim, J. Cryst. Growth **220**, 494–500 (2000).
[57] J. Q. Hu, Q. Li, X. M. Meng, C. S. Lee, and S. T. Lee, J. Phys. Chem. B **106**, 9536–9539 (2002).
[58] X. C. Wu, W. H. Song, W. D. Huang, M. H. Pu, B. Zhao, Y. P. Sun, and J. J. Du, Chem. Phys. Lett. **328**, 5–9 (2000).
[59] J. Zhang and L. D. Zhang, Solid State Commun. **122**, 493–496 (2002).
[60] G. Gundiah, A. Govindaraj, and C. N. R. Rao, Chem. Phys. Lett. **351**, 189–194 (2002).
[61] G. X. Wang, J. Park, X. Y. Kong, P. R. Wilson, Z. X. Chen, and J. H. Ahn, Cryst. Growth Des. **8**, 1940–1944 (2008).
[62] D. Dohy, G. Lucazeau, and A. Revcolevschi, J. Solid State Chem. **45**, 180–192 (1982).
[63] R. Rao, A. M. Rao, B. Xu, J. Dong, S. Sharma, and M. K. Sunkara, J. Appl. Phys. **98**, 094312 (2005).
[64] J. Y. Li, X. L. Chen, Z. Y. Qiao, M. He, and H. Li, J. Phys: Condens. Mater. **13**, L937–L941 (2001).
[65] K. W. Chang and J. J. Wu, Appl. Phys. A **76**, 629–631 (2003); Appl. Phys. A **77**, 769–774 (2003).
[66] L. Dai, X. L. Chen, X. N. Zhang, A. Z. Jin, T. Zhou, B. Q. Hu, and Z. Zhang, J. Appl. Phys. **92**, 1062–1064 (2002).
[67] D. P. Yu, J. L. Bubendorff, J. F. Zhou, Y. Leprince-Wang, and M. Troyon, Solid State Commun. **124**, 417–421 (2002).
[68] H. J. Chun, Y. S. Choi, S. Y. Bae, H. W. Seo, S. J. Hong, J. Park, and H. Yang, J. Phys. Chem. B **107**, 9042–9046 (2003).
[69] X. Xiang, C. B. Cao, and H. S. Zhu, J. Cryst. Growth **279**, 122–128 (2005).
[70] K. F. Cai, S. Shen, C. Yan, and S. Bateman, Curr. Appl. Phys. **8**, 363–366 (2008).
[71] C. H. Liang, G. W. Meng, G. Z. Wang, Y. W. Wang, L. D. Zhang, and S. Y. Zhang, Appl. Phys. Lett. **78**, 3202–3204 (2001).
[72] Z. R. Dai, Z. W. Pan, and Z. L. Wang, J. Phys. Chem. B **106**, 902–904 (2002).
[73] J. H. Zhan, Y. Bando, J. Q. Hu, F. F. Xu, and D. Golberg, Small **1**, 883–888 (2005).
[74] E. Auer, A. Lugstein, S. Loffler, Y. J. Hyun, W. Brezna, E. Bertagnolli, and P. Pongratz, Nanotechnology **20**, 434017 (2009).
[75] L. C. Tien, C. H. Ho, X. T. Yao, and J. R. Cai, Appl. Phys. A **102**, 105–108 (2011).
[76] (a) K. W. Chang and J. J. Wu, Adv. Mater. **16**, 545 (2004). (b) K. W. Chang and J. J. Wu, J. Phys. Chem. B **108**, 1838–1843 (2004).
[77] N. H. Kim, H. W. Kim, C. Seoul, and C. Lee, Mater. Sci. Eng. B **111**, 131–134 (2004).
[78] S. Sharma and M. K. Sunkara, J. Am. Chem. Soc. **124**, 12288–12293 (2002).
[79] F. Zhu, Z. X. Yang, W. M. Zhou, and Y. F. Zhang, Appl. Surf. Sci. **252**, 7930–7933 (2006).
[80] F. Zhu, Z. X. Yang, W. M. Zhou, and Y. F. Zhang, Solid State Commun. **137**, 177–181 (2006).
[81] T. I. Shin, H. J. Lee, W. Y. Song, S.-W. Kim, M. H. Park, C. W. Yang, and D. H. Yoon, Nanotechnology **18**, 345305 (2007).
[82] K. Shimamura, E. G. Villora, T. Ujiie, and K. Aoki, Appl. Phys. Lett. **92**, 201914 (2008).
[83] Y. P. Song, H. Z. Zhang, C. Lin, Y. W. Zhu, G. H. Li, F. H. Yang, and D. P. Yu, Phys. Rev. B **69**, 075304 (2004).
[84] L.-W. Chang, T.-Y. Lu, Y.-L. Chen, J.-W. Yeh, and H. C. Shih, Mater. Lett. **65**, 2281–2283 (2011).
[85] R. Jangir, S. Porwal, P. Tiwari, P. Mondal, S. K. Rai, T. Ganguli, S. M. Oak, and S. K. Deb, J. Appl. Phys. **112**, 034307 (2012).
[86] D. P. Yu, J. L. Bubendorff, J. F. Zhou, Y. Leprince-Wang, and M. Troyon, Solid State Commun. **124**, 417–421 (2002).
[87] Z. Li, B. Zhao, P. Liu, and Y. Zhang, Microelectron. Eng. **85**, 1618–1620 (2008).
[88] E. G. Villora, T. Atou, T. Sekiguchi, T. Sugawara, M. Kikuchi, and T. Fukuda, Solid State Commun. **120**, 455 (2001).
[89] P.-C. Chang, Z. Fan, W.-Y. Tseng, A. Rajagopal, and J. G. Lu, Appl. Phys. Lett. **87**, 222102 (2005).
[90] Y. Huang, S. Yue, Z. Wang, Q. Wang, C. Shi, Z. Xu, X. D. Bai, C. Tang, and C. Gu, J. Phys. Chem. B **110**, 796–800 (2006).
[91] S. P. Arnold, S. M. Prokes, F. K. Perkins, and M. E. Zaghloul, Appl. Phys. Lett. **95**, 103102 (2009).
[92] N. D. Cuong, Y. W. Park, and S. G. Yoon, Sens. Actuators B **140**, 240–244 (2009).
[93] L. Mazeina, F. K. Perkins, V. M. Bermudez, S. P. Arnold, and S. M. Prokes, Langmuir **26**, 13722–13726 (2010).
[94] P. Feng, J. Y. Zhang, Q. H. Li, and T. H. Wang, Appl. Phys. Lett. **88**, 153107 (2006).
[95] L. Li, E. Auer, M. Y. Liao, X. S. Fang, T. Y. Zhai, U. K. Gautam, A. Lugstein, Y. Koide, Y. Bando, and D. Golberg, Nanoscale **3**, 1120–1126 (2011).

